LIMNOLOGY and OCEANOGRAPHY

Use of ^{223}Ra and ^{224}Ra as chronometers to estimate the residence time of Amazon waters on the Brazilian continental shelf

Morgane Léon [ORCID],[1]* Pieter van Beek [ORCID],[1] Jan Scholten [ORCID],[2] Willard S. Moore [ORCID],[3] Marc Souhaut,[1]
Joselene De Oliveira,[4] Catherine Jeandel,[1] Patrick Seyler,[5] Julien Jouanno[1]

[1]Laboratoire d'Etudes en Géophysique et Océanographie Spatiales (LEGOS), Université de Toulouse, CNES/CNRS/IRD/Université Toulouse III Paul Sabatier, Toulouse, France
[2]Institute of Geosciences, Kiel University, Kiel, Germany
[3]School of Earth, Ocean and Environmental Science, University of South Carolina, Columbia, South Carolina
[4]Department of Environmental Radiometrics (LRA), Instituto de Pesquisas Energéticas e Nucleares (IPEN), Sao Paulo, Brazil
[5]HydroSciences Montpellier (HSM), IRD/CNRS/University Montpellier, Montpellier, France

Abstract

When rivers mix into the ocean, radium isotopes are released into the dissolved phase allowing us to apply these isotopes as powerful tracers of river plumes spreading into the ocean. We report ^{223}Ra and ^{224}Ra radium activities that were determined in the Amazon River mouth and along the Amazon plume that extends off the coasts of Brazil and French Guyana into the Atlantic Ocean. We summarize ^{223}Ra and ^{224}Ra data from AmasSeds (1991), AMANDES (GEOTRACES process study GApr01; 2007–2008) and M147 (2018) projects, which were conducted in different seasons corresponding to different Amazon discharge rates. We determined the ^{224}Ra$_{ex}$/^{223}Ra activity ratios (AR) along the Amazon plume to derive apparent ages and to estimate the residence time of the Amazon waters on the Brazilian continental shelf. Our data suggest that it takes 9–14 d for the Amazon waters to reach the northern continental shelf off French Guyana and 12–21 d to reach the eastern part of the Brazilian continental shelf. These time scales are in good agreement with those derived from a high-resolution numerical simulation of the regional ocean dynamics. We do not find any relationship between the discharge rate of the Amazon River and the residence time of the waters on the Brazilian continental shelf, suggesting that the residence time of the Amazon waters is primarily driven by the ambient northwestward current. Using the apparent ages along the plume, we estimate an average velocity of 26 cm s^{-1} for the northward transport of the Amazon waters on the continental shelf.

The Amazon River, the largest freshwater input into the oceans, discharges into the Atlantic Ocean with an average flowrate of 205,000 m^3 s^{-1}, representing 17% of the world's river input (Callède et al. 2010). This flow displays a large

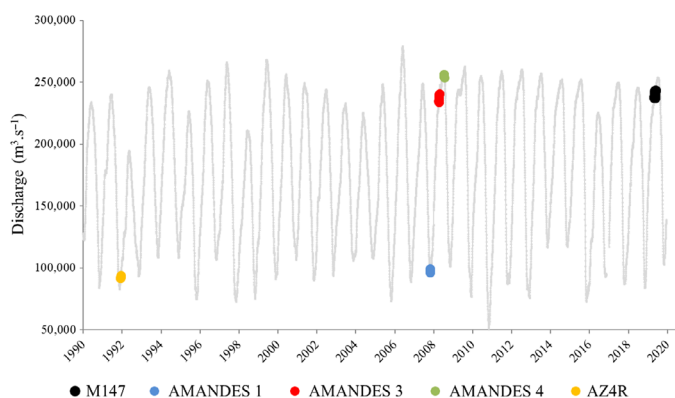Additional Supporting Information may be found in the online version of this article.

seasonal variability, ranging from 80,000 m^3 s^{-1} in October–December to 250,000 m^3 s^{-1} between April and June at Óbidos station (1.9°S, 55.5°W) (Fig. 1; HYBAM 2020). The Amazon mouth is bordered by a multitude of mangroves and channels, giving it a complex shape. South of the island of Marajo, the Para River shares a common mixing zone with Amazon River but a different watershed. The Para River is composed of 30% Amazon River water but carries less than 5% of the discharge of the Amazon River (Callède et al. 2010). The Amazon River waters flow onto the very flat and shallow Brazilian continental shelf, which extends northeast 250 km away from the mouth. Offshore, the plume extends thousands of kilometers (e.g., Muller-Karger et al. 1988; Hu et al. 2004) and thus impacts the freshwater budget of the tropical Atlantic Ocean (Coles et al. 2013). The Amazon plume flowing on the continental shelf is characterized by a variable but thin surface layer (5–10 m thick) of low-salinity water that creates a barrier to vertical mixing (Grodsky et al. 2012; Coles et al. 2013; Reul et al. 2014). Approximately 1.12 × 10^9 tons

Fig. 1. Discharge of the Amazon River (m^3 s^{-1}) measured at Obidos station (HYBAM, between January 1990 and January 2020). The discharge corresponding to (1) ARZ4 is shown in orange; (2) AMANDES 1, AMANDES 3, and AMANDES 4 in blue, red, and green, respectively; and (3) M147 in black.

of suspended particles (Meade et al. 1985) and 2.3×10^8 tons of dissolved material are transported yearly (Livingstone 1963; Gibs 1972; Armijos et al. 2020) into the Atlantic Ocean by the Amazon River. Part of this material accumulates on the shelf, while the rest is exported offshore. The particles that settle on the shelf move horizontally and vertically. Moore et al. (1996) estimated that 3.4×10^{10} tons of sediment was resuspended on the continental shelf every year.

The fate of the Amazon plume along the Brazilian shelf is controlled by various energetic forcing factors, acting over a broad range of spatial and temporal scales, including tides, winds, and currents. The North Brazil Current (NBC) is fed by the South Equatorial Current, which flows northwestward along the Brazilian coast at rates of 13–36 Sv (Johns et al. 1998). During most of the year, the NBC drives the Amazon plume toward the northwest along the coasts of French Guiana (Baklouti et al. 2007) and Venezuela (Moore and Todd 1993), before reaching the Caribbean Sea (Moore et al. 1986). Between late summer and January, a retroflexion of the plume takes place above the Demerara Plateau offshore the French Guiana shelf, between about 5°N and 10°N, deflecting these waters southeastward toward the Atlantic Ocean interior (Johns et al. 1990). Ruault et al. (2020) recently demonstrated the importance of the tidal effects in the general circulation of the Amazon plume on the continental shelf. Tidal effects cause a weakening of the mean currents in shallow areas, a process that favors the dispersion of the low-salinity waters in the mouth region. Furthermore, tides favor the spreading of the freshwater plume offshore and toward the northwest along the northern coasts of South America. Winds also constitute an important factor influencing the plume dispersion. During the first part of the year (January–May), the strong winds blowing southwestward tend to inhibit the spreading of the plume, whereas northwestward winds blowing between June and November enhance the

along-shelf flow (Geyer et al. 1996). Lentz (1995) concludes that the along-shelf current variability of the plume is thus strongly influenced by wind stress, on timescales of days to weeks. Tidal effects as well as wind stress may thus have an influence on the residence time of the plume on the continental shelf.

In the early 1990s, the AmasSeds (A Multidisciplinary Amazon Shelf SEDiment Study; 1989–1991) program was one of the first interdisciplinary projects conducted along the Brazilian Shelf. It was designed to study the discharge of water, solutes and particulate matter associated with the Amazon River and to evaluate its impact on the coastal environment (Nittrouer et al. 1995). It was shown that the Amazon delta consisted of a large mixing zone where many chemical reactions took place as a result of (1) the large amounts of dissolved chemical elements and suspended particles transported by the river, (2) salinity gradients that promoted the release of chemical elements from particles due to increased ionic stress, (3) interactions with bottom sediments due to the shallow shelf and spring tides that favor sediment resuspension (Kineke et al. 1996), and (4) upwelling of deeper waters at the shelf break created by the large volume of river discharge (Geyer et al. 1996). Most of the annual sediment discharge (35–70%) was shown to accumulate on the shelf (Kuehl et al. 1986; Nittrouer et al. 1986), while 7–17% was advected toward the northwest with <5% being transported by the low salinity surface plume (Kineke et al. 1996). Smith and Demaster (1996) showed that the Brazilian continental shelf was a region of high primary production—with significant spatial variability—that results from the combination of riverine, upwelling nutrient inputs, and irradiance availability offshore. Yet the origin of the nutrients fertilizing the shelf is not clear. Smith and Demaster (1996) suggested that excess of macronutrients in the shelf could be explained by resuspension at shallow depths while other studies concluded that the upwelling provided compelling evidence that the outer shelf algal blooms were supported primarily by the shoreward flux of nutrients from offshore, subsurface waters (Smoak et al. 1996; Demaster and Pope 1996). Using satellite data—when cloud cover permitted—Müller-Karger et al. (1989) investigated the Amazon plume dispersion through pigment concentrations. They reported a seasonal increase of plankton in the low salinity plume between July and November, and traced it as far as the Caribbean Sea. The Amazon shelf is thus a marine environment where primary production and silica production are high, primarily as a result of river-induced upwelling at the shelf break (Nittrouer and DeMaster 1996). As a consequence, this region is characterized by significant uptake of atmospheric CO_2 and has a significant impact on the carbon budget of the tropical Atlantic (Lefévre et al. 2010; Ibánhez et al. 2016).

Along the salinity gradient, many chemical reactions thus take place that may impact the biogeochemical content of the plume that may, in turn, impact the primary production on

the continental shelf as well as the chemical composition of Atlantic waters. The rate of the chemical reactions taking place along the plume entering into Atlantic Ocean waters thus controls the intensity of the chemical fluxes released along the continent shelf. Knowledge of the residence time of the waters on the Brazilian continental shelf is thus critical to better constrain the transfer of chemical species at this specific continental-ocean interface and to evaluate how these fluxes may impact the chemical composition of the Atlantic Ocean and the oceanic biological carbon pump.

With four natural isotopes with different half-lives ([224]Ra, 3.66 d; [223]Ra, 11. 4 d; [228]Ra, 5.75 yr; [226]Ra, 1600 yr), radium is a tracer that allows us to study processes on diverse spatial and temporal scales from in-situ data. These isotopes have been widely used to study the fate of river plumes entering into the oceans (Key et al. 1985; Moore et al. 1995, 1986; Moore and Krest 2004; Peterson et al. 2008). In freshwater, most of the radium is adsorbed onto suspended particles. When freshwater mixes with saltwater, radium desorbs from particles due to increased ionic competition and is thus released into the dissolved form (Moore et al. 1995). Radium isotopes can be used to trace the fate of the plume entering into the ocean and also as chronometers to estimate the water residence time (Moore and Krest 2004; Rousseau et al. 2015). In the framework of the TTO program (Transient Tracer in the Ocean), Key et al. (1985) quantified the flux of [226]Ra and [228]Ra in the Amazon mixing zone and highlighted the importance of radium desorption from river-borne sediment. This study concluded that the dissolved radium flux associated with the river water was five times less than the radium flux released by river-borne suspended particles. Moore et al. (1986) showed that the [228]Ra/[226]Ra ratio was a good tracer for Amazon waters in the Atlantic Ocean and reported relatively high [228]Ra/[226]Ra ratios of Amazon plume origin thousands of kilometers from the riverine or shelf source. The efficiency of the radium chronometers was illustrated during AMANDES cruise by the work of Rousseau et al. (2015). By coupling Ra isotopes to the dissolved and particulate Nd isotopic compositions, these authors have determined that neodymium was released from lithogenic particles at relatively short time scale (3 weeks).

In this study, we estimate apparent water ages and transport velocities derived from the analysis of short half-life radium isotopes at the mouth of the Amazon River and on the Brazilian continental shelf. We also aim to evaluate the impact of the different hydrographic regimes on the residence time of the Amazon waters on the Brazilian continental shelf.

Material and methods
Field studies
We report radium activities determined in the framework of three different projects that were conducted in the Amazon River mouth and on the Brazilian continental shelf (Table 1).

We present a set of samples from the AmasSeds project collected during the AZ4R cruise (November–December 1991) where surface samples were collected between the Amazon mouth and the Caribbean Sea. While [224]Ra, [226]Ra, and [228]Ra activities have been reported in this region in a previous study (Moore et al. 1995), the AZ4R cruise provided the earliest samples measured for [224]Ra and [223]Ra data offshore the Amazon mouth. The second set of samples originated from the AMANDES project (2007–2008); (Le Bars et al. 2010; Rousseau et al. 2015; Prestes et al. 2018). These latter campaigns aimed at better understanding the physico-chemical exchange processes that take place in the Amazon delta and along the Brazilian continental shelf and at evaluating the impact on the chemical composition of the Atlantic Ocean waters. One campaign was conducted offshore the coast of French Guiana to investigate the fate of Amazon waters within the retroflexion (AMANDES 1, 24 October–01 November 2007) and two campaigns were conducted on the Brazilian shelf (AMANDES 3, 06–18 April 2008 and AMANDES 4, 10–20 July 2008). Finally, the last set of samples was more recently collected in the framework of the M147 cruise conducted along the entire Brazilian shelf (30 April–17 May 2018). Samples collected during this latter cruise, in the south of the Amazon River mouth, were recently used to show the importance of the lateral carbon flux from mangroves to the coastal ocean (Cabral et al. 2021).

All these campaigns were conducted at different times of the year and thus cover different hydrographic regimes of the Amazon River (high vs. low discharge; Table 1; Fig. 1). AMANDES 1 and AZ4R cruises were conducted during low discharge of the Amazon River, at a period when the retroflexion of the plume into the interior of the Atlantic Ocean took place. The Amazon discharge was higher during AMANDES 3 and M147 cruises, whereas AMANDES 4 was conducted during high discharge (no retroflexion at these times). Figure 2 shows the sample locations of the five campaigns.

Sample collection
During AZ4R cruise, surface (~2 m) water samples (96–317 liter) were collected from the bow pump of the R/V COLUMBUS ISELIN into plastic barrels (Supplementary Information Table S1). If the water was clear and low in suspended solids, it was filtered directly through a column of MnO_2-coated fibers (i.e., Mn-fiber) to quantitatively remove radium (Moore 1976). Samples that contained significant suspended solids were first passed through a 1 μm cartridge filter. In some cases, highly turbid samples were allowed to settle 10–20 h before filtering. Freshwater end member samples were passed through a 0.45 μm filter after passing the 1 μm cartridge filter. To test the recovery of Ra on the Mn-fiber, we placed a second column of Mn-fiber in series with the first column for a number of samples. In no case did we record more than 3% of the Ra activity on the second column relative to the first. Samples

Table 1. Information on the different cruises reported in this study. The discharge of the Amazon River ($m^3 s^{-1}$) is given by HYBAM (2020) at Obidos station. Estimates of the North Brazilian Current (NBC) flow are reported in Sverdrups ($10^6 m^3 s^{-1}$) for the appropriate time of the year according to Nittrouer et al. (1995).

| | Date | | | | NBC | No. of |
| | Start | End | Location | Discharge ($m^3 s^{-1}$) | transport (Sv) (approximation) | surface samples |
Cruise						
AZ4R	27 Nov 1991	04 Dec 1991	Between the Amazon mouth and the Caribbean Sea	92,000–94,000	22 (+ Retroflexion)	32
AMANDES 1	24 Oct 2007	01 Nov 2007	Offshore French Guiana	95,800–99,000	22 (+ Retroflexion)	18
AMANDES 3	06 Apr 2008	18 Apr 2008	Amazon mouth and Brazilian continental shelf	233,800–240,400	10	14
AMANDES 4	10 Jul 2008	20 Jul 2008	Amazon mouth and Brazilian continental shelf	253,600–256,200	20 (+ Beginning of retroflexion)	20
M147	30 Apr 2018	17 May 2018	Amazon mouth and Brazilian continental shelf	216,500–237,500	10	63

to measure salinity by salinometer were taken from the large volume homogenized samples before radium analyses. In regions of strong salinity gradients, the salinity of the pumped Ra samples may not match the salinity of the CTD taken at different time.

During AMANDES cruises, large volumes of water were collected using the ship seawater intake (~2 m depth) and were filled into 20-liter cubitainers (Supplementary Information Table S2). As a comparison, surface water samples were also occasionally collected using Niskin bottles and a clean, all-Teflon double bellow ASTI pump (designed to collect water samples for trace metal analysis). Two surface samples were collected using a hand pump from a rubber boat during AMANDES 1 cruise within the salinity gradient ($S = 0$–10) of the Oyapock river located at the border between Brazil and French Guiana. During AMANDES 1 and AMANDES 4 cruises, samples were also collected at different depths to establish vertical profiles. All water samples were filtered using 1-μm filter cartridges. During filtration, the water volume was quantified using a flowmeter. The filtered water was stored in 20-liter cubitainers and then passed through Mn fibers at a flow rate <1 L min^{-1} (Moore and Reid 1973; Moore 1976). Prior to the analyses of short-lived Ra isotopes, the Mn-fibers were rinsed with MilliQ water and partially dried in order to obtain a fiber : water ratio of 1 : 1 (Sun and Torgersen 1998). Sea-surface salinity was obtained from the salinometer of the ship, and with CTD systems for deep samples.

During M147 cruise, surface seawater samples (~2 m water depth) were collected using a WASP-5 underwater pump (Supplementary Information Table S3). Between 16 and 236 liter of water was filled into barrels. Thereafter the water was filtered (1 μm cartridge filter) and Mn-fibers with a flow rate ≤1 L min^{-1} to adsorb Ra. The Mn-fibers were washed salt-free using radium-free tap water. Before analyses, the Mn-fibers were partially dried (water content between 50% and

100%). Short-lived Ra isotopes were then analyzed on-board the ship.

Analysis

The very first measurements of ^{223}Ra in the open ocean were made during AZ4R cruise. The counting system was a primitive version of the electronic package that became the RaDeCC system (Moore and Arnold 1996, *see* below). Selected samples were recounted every 2–4 d to ensure that the activities followed the expected decay curves; they generally did so within ±15%. However, due to occasional erratic behavior of the counter and uncertainty in standard calibration, we place one sigma error of ±20% error on the ^{224}Ra measurements and ±30% error on the ^{223}Ra measurements.

During AMANDES and M147 cruises, short-lived ^{223}Ra and ^{224}Ra activities were determined using a Radium Delayed Coincidence Counter (RaDeCC; Moore 2008; Moore and Arnold 1996). A first counting session was run directly after sample collection to determine the total ^{224}Ra and ^{223}Ra activities. The Mn-fibers were analyzed again 3 weeks after sampling to determine the ^{224}Ra activities supported by ^{228}Th. These supported activities were then subtracted from the total ^{224}Ra activities to determine excess ^{224}Ra (denoted ^{224}Ra$_{ex}$). To determine the ^{223}Ra activity supported by ^{227}Ac, the samples collected during the AMANDES cruises were analyzed again 3 months after sampling. ^{227}Ac activities were often below the detection limit or <0.2 dpm 100 L^{-1}, which is within the uncertainties of the ^{223}Ra activities. This means the ^{223}Ra was not significantly impacted by ^{227}Ac in the water column. We therefore neglect ^{227}Ac and simply report total ^{223}Ra and ^{224}Ra$_{ex}$/^{223}Ra activity ratios (AR) for each cruise in Supplementary Tables S1–S3. Error propagation calculations followed Garcia-Solsona et al. (2008).
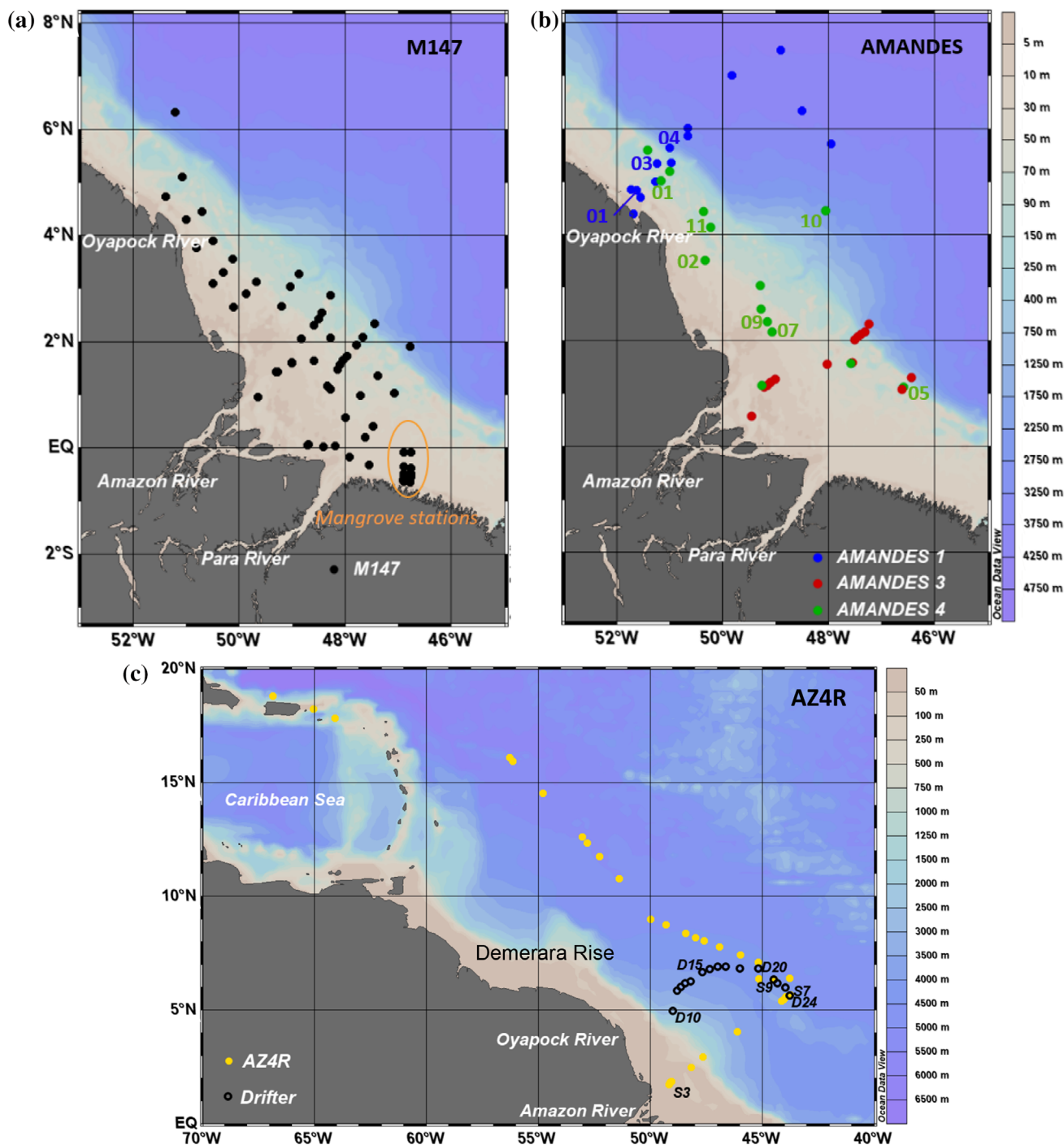
Fig. 2. Location of the samples collected in the different cruises (surface samples). M147 stations (2018) are on panel (**a**), AMANDES stations (2007–2008) are on panel (**b**) and AZ4R stations (1991) are on panel (**c**). Samples collected near mangroves are circled in orange. Numbers on panel (**b**) represent stations where vertical profiles were made. A drifter was released near Sta. 3 (S3) during AZ4R. Open circles indicate the track of the drifter, with numbers adjacent to the drifter locations (D) indicating the number of days elapsed since release. The ship and drifter paths intersected at Sta. 9 (drifter day 21) and Sta. 7 (drifter day 24). The gray and blue shadings represent the bathymetry.

Modeling

High-resolution numerical simulations were made based on the NEMO 3.6 ocean model (Madec 2014), a model specially designed to reproduce the dynamics on the Brazilian shelf and its interaction with the large-scale oceanic circulation. The model description and validation of the plume properties and dynamics can be found in Ruault et al. (2020). The resolution of the model is refined to 1/36° (~2.7 km horizontal
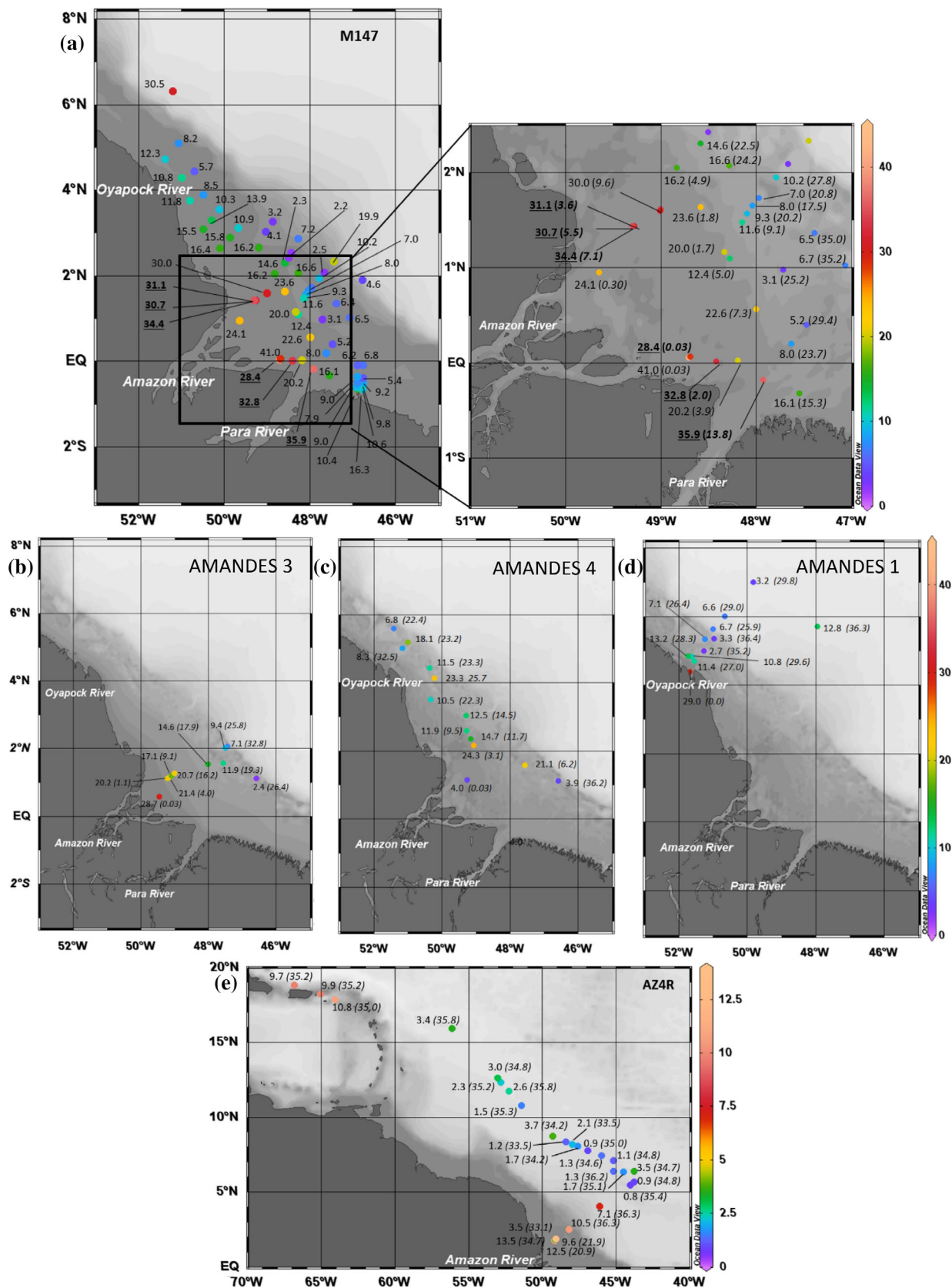
Fig. 3. $^{224}Ra_{ex}/^{223}Ra$ activity ratios (color scale and values near sample locations) determined during (**a**) M147, (**b**) AMANDES 3, (**c**) AMANDES 4, (**d**) AMANDES 1, and (**e**) AZ4R cruises offshore the Amazon mouth. Salinity is shown under parentheses. The values in the Amazon mouth used to determine the initial $^{224}Ra_{ex}/^{223}Ra$ ratio are underlined.

resolution) in the area under study (3.5°S–10°N and 53°W–42.5°W). The model is forced using interannually varying atmospheric forcing (Dussin et al. 2016). It includes the interannual variability of the Amazon and Orinoco Rivers derived from the HYBAM database, while climatological runoff from Dai and Trenberth (2002) are prescribed otherwise (e.g., for the Para River).

The transport of the plume and advection time in the model are investigated from a Lagrangian perspective. Parcels are launched at the river mouth and traced forward in time during 50 d using the Lagrangian tool ARIANE (Blanke and Raynaud 1997). Water parcels (99,100 in total) are seeded at 5 m depth each day from January 2005 to December 2015, at each model grid points located along a section within the Amazon plume, where salinities are 0 (between 50°W–1°N and 49.2°W–0.2°S). The age counter begins when the particles enter in waters with a salinity greater than 1. Ages are mapped daily on a regular grid of $0.2° \times 0.2°$ resolution and are then averaged over the dates of the different cruises.

Results

Distribution of salinity and Ra isotopes along the Brazilian shelf

The Amazon River largely controls the salinity distribution on the Brazilian continental shelf (Supplementary Information Fig. S1). The low salinity plume can be observed up to 260 km northwest of the Amazon mouth during M147 cruise and relatively low salinities (e.g., 34.8) are also observed as far as 12.5°N during AZ4R cruise (Supplementary Information Fig. S1e). A salinity of 36.2 is found near the continental shelf break, in front of the mouth, which is close to the salinity of Atlantic Ocean open surface waters (Geyer et al. 1996). Coastal water samples collected during M147 cruise south of the Para River display salinities ranging from 27.1 to 33.1 (Supplementary Information Fig. S1a).

The distributions of $^{224}Ra_{ex}$ and ^{223}Ra activities during each cruise are shown in Supplementary Figs. S2 and S3. At salinities below 1, Ra activities are very low (e.g., 0.6 dpm 100 L^{-1} for $^{224}Ra_{ex}$ and 0.1 dpm 100 L^{-1} for ^{223}Ra during AMANDES 3 cruise). During AMANDES 3 cruise, ^{223}Ra activities are below the detection limit at a salinity of 0.03 near the Amazon River mouth. Then, $^{224}Ra_{ex}$ (and ^{223}Ra) activities increase considerably with increasing salinity in the first kilometers past the Amazon mouth. The highest $^{224}Ra_{ex}$ activity (156 dpm 100 L^{-1}; Supplementary Information Fig. S2) determined during the M147 cruise—which provides the best spatial resolution on the continental shelf among the five campaigns—is found at a salinity of 9.6. Here, we observe the second highest ^{223}Ra activity reported during this cruise (5.18 dpm 100 L^{-1}; Supplementary Information Fig. S3). These highest radium activities are generally found on the continental shelf at stations where significant mixing occurred between freshwater from the Amazon River and seawater (salinity range ~ 4–20;

Supplementary Information Figs. S2–S4). $^{224}Ra_{ex}$ (and ^{223}Ra) activities then progressively decrease when salinities become higher (Supplementary Information Fig. S4).

In the southern part of the Brazilian continental shelf, the Ra activities range from 1.1 to 118 dpm 100 L^{-1} for $^{224}Ra_{ex}$ and from 0.2 to 6.9 dpm 100 L^{-1} for ^{223}Ra during all campaigns. Coastal samples collected during M147 cruise in the southern part of the continental shelf, near mangroves, display maximum Ra activities of 42 and 3.2 dpm 100^{-1} L, for $^{224}Ra_{ex}$ and ^{223}Ra, respectively. Offshore the continental shelf, Ra activities are very low, but still significantly higher than open ocean waters. Both ^{223}Ra and $^{224}Ra_{ex}$ activities follow the same pattern on the continental shelf during all campaigns. This is also shown by the fairly good correlation between ^{223}Ra and $^{224}Ra_{ex}$ activities (Supplementary Information Fig. S5). During AMANDES 1 cruise, the increase of Ra activities with increasing salinity (0–20) was also observed in the Oyapock river mouth; the highest Ra activity (83 dpm 100 L^{-1} for $^{224}Ra_{ex}$ and 5.2 dpm 100 L^{-1} for ^{223}Ra) was found at a salinity of 20, but the sampling resolution was low within the salinity gradient of that river.

Distribution of $^{224}Ra/^{223}Ra$ activity ratios in the Amazon River plume

The distribution of $^{224}Ra/^{223}Ra$ AR during each cruise is shown in Fig. 3. As expected from the distribution of the ^{223}Ra and $^{224}Ra_{ex}$ activities, the highest AR are not found at the Amazon mouth, but on mid-shelf. From there, the ARs gradually decrease with increasing distance offshore. The ARs determined in both M147 and AMANDES cruises range from 2.2 to 41. In the first 150 km around the Amazon River mouth, relatively high ARs (> 15) are found during AMANDES cruises; because of the higher sampling resolution during M147 cruise, more ARs are available in the salinity gradient, with several ARs > 30 (Fig. 3a). ARs then gradually decrease offshore, with a steeper gradient northeast than northwest. For example, during the AMANDES 4 cruise, AR was 3.9 at 80 km from the mouth (northeastward) and was 6.8 at 580 km (northwestward). Samples collected near mangroves during M147 cruise display variable but relatively high ARs, ranging from 5.4 to 16 (Fig. 3a).

We note, however, that several ARs do not follow the smooth decrease as a function of increased distance from the mouth. Such pattern was observed during AMANDES 4 cruise where two samples display relatively high ARs, although they are located relatively far from the Amazon mouth. Other examples are also given during the M147 cruise, such as sample M147-59 located at the shelf break (47.5°W, 2.3°N) with a relatively high AR of 20 or M147-100 located offshore the French Guiana shelf (51.2°W; 6.3°N) with an AR of 30. Samples from AZ4R usually present an overall decreasing trend in the ARs with increasing distance from the mouth, with the exception of the three northern
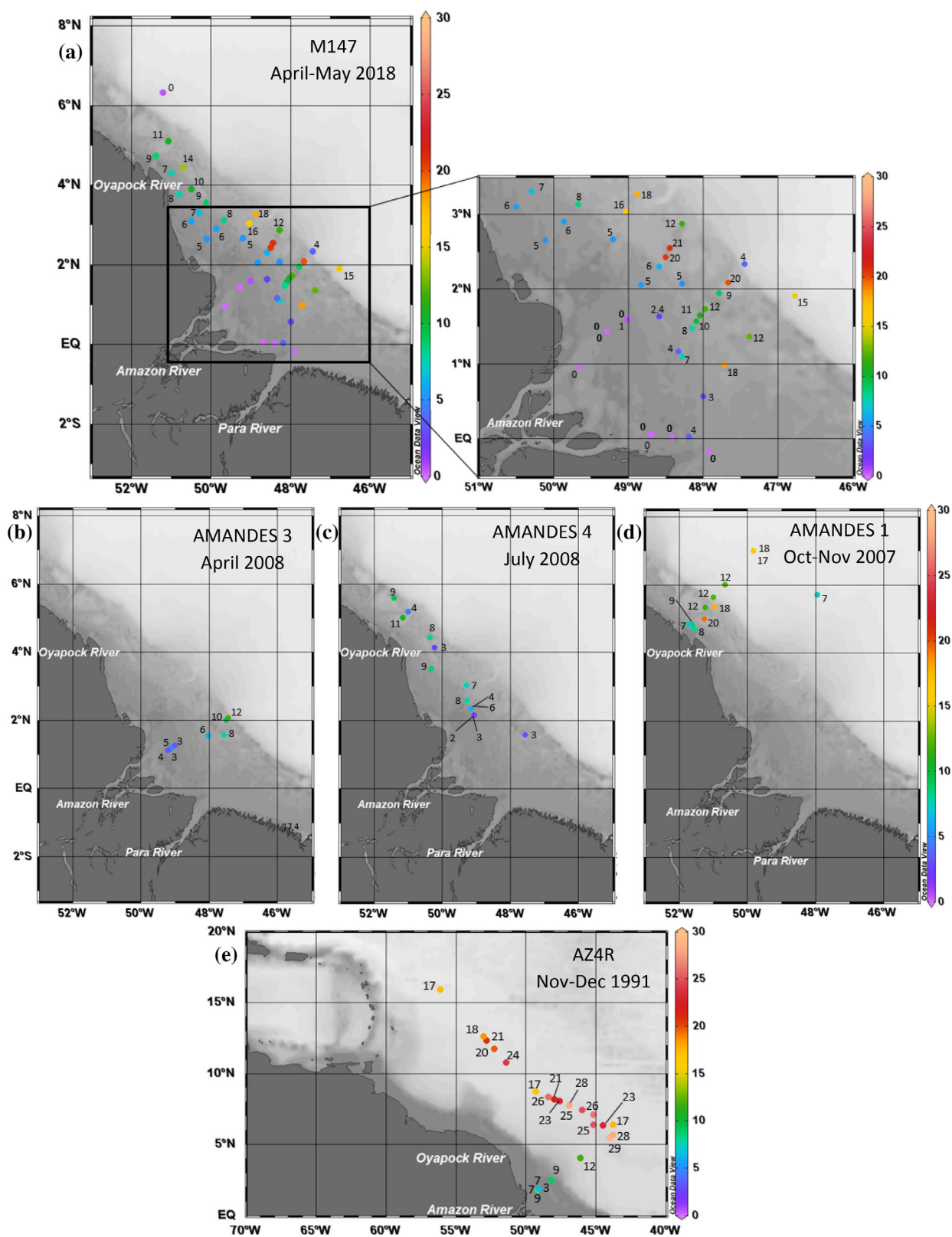
Fig. 4. Apparent ages in days (color scale and values near sample locations) determined during (**a**) M147, (**b**) AMANDES 3, (**c**) AMANDES 4, (**d**) AMANDES 1, and (**e**) AZ4R cruises on the Brazilian continental shelf, considering an initial activity ratio $^{224}Ra_{ex}/^{223}Ra$ of 32. Stations with salinity of less than 0.3 were excluded from the age calculation.

samples collected near the Caribbean islands that display high AR (9.7–11).

Discussion

Distribution of salinity and Ra isotopes

The salinity distribution above the Brazilian continental shelf clearly indicates an advection of the Amazon waters toward the northwest along the Brazilian and French Guiana coasts. Relatively low surface salinity is observed south of the Para River and may indicate an additional input of freshwater—not related to the Amazon River—which may originate from the numerous littoral rivers flowing into these coastal waters (Marapanim, Maracana, Gurupi Rivers) and potentially also submarine groundwater discharge. Overall, all campaigns give a consistent picture of the spreading of the Amazon River plume toward northeast and northwest.

Radium activities increase within the salinity gradient as a result of the release of radium from suspended particles into the dissolved phase due to increased ionic competition. Ra activities then decrease with increasing salinity and with distance from the mouth as a consequence of radioactive decay and mixing with seawater (Supplementary Information Fig. S4). The global decreasing trend—once desorption of radium is achieved—suggests that radium may be considered as a chemically conservative tracer at salinities above 10–20. As for salinity, $^{224}Ra_{ex}$ and ^{223}Ra activities indicate a clear advection of the Amazon plume on the continental shelf that flows northward. Further offshore, the Ra activities determined during the AMANDES 1 cruise can be related to the Amazon plume that first flows northward along the coast of French Guiana and then eastward into the Atlantic Ocean due to the retroflexion that takes place at that time.

The AR distribution observed during the different cruises (Fig. 3) agrees with the circulation patterns in this area (i.e., waters flowing northward along the coast) and allows us to presume that the main source of Ra comes from the Amazon mixing zone. However, during AZ4R cruise, the three most northerly samples do not reflect any influence of the Amazon plume at this latitude, but rather indicate that coastal waters are impacted by the shallow sediments that release Ra in this region. A salinity anomaly indicator was proposed as the difference between the salinity of the sample and the average salinity of the Atlantic Ocean (i.e., 36.2). These anomalies are reported, as well as the AR's measured in this work, as function of offshore distance (Supplementary Information Fig. S6). The overall view is that the AR decrease with increasing distance from the Amazon mouth, in relationship with the decrease in the salinity anomaly (as a consequence of the mixing with Atlantic Ocean waters). This pattern highlights that the AR is in most cases tightly connected to the Amazon plume. Therefore, we assume that the ARs change only by radioactive decay and mixing with open oceans waters and

can thus be used to derive apparent water ages. The same global decreasing trend of AR and salinity anomalies with increasing distance from the Amazon mouth can also be observed during M147, AMANDES 4, and AZ4R cruises, although several outliers can be found (Supplementary Information Fig. S6).

In a previous study, Moore et al. (1995) demonstrated that the primary source of ^{224}Ra to the Amazon shelf was from resuspension of the fluid mud layer at mid-shelf, and not from the river itself. Presumably, ^{223}Ra is derived from the same source. The resuspension effect is usually more pronounced during periods of rising or high discharge of the Amazon River but also during spring tides; both processes increase the mixing in the entire water column. Several vertical profiles of Ra were collected during AMANDES 1 and AMANDES 4 cruises (Supplementary Information Table S4) to investigate the vertical distribution of Ra and to evaluate the possible impact of resuspended particles on the dissolved Ra activities in surface waters. In most cases, a clear Ra enrichment was observed in the low-salinity surface waters of the Amazon plume (Supplementary Information Fig. S7a–g). Below the plume, the Ra activities were low and tended to increase again close to the bottom. The combined effects of the stratification that results from the large salinity difference between the Amazon plume and waters from below and the relatively high velocity of the plume (Geyer and Kineke 1995) may thus limit the impact of sediment resuspension on the Ra signature of the plume. At two stations, however, we found higher $^{224}Ra_{ex}$ and ^{223}Ra below the Amazon plume (Supplementary Information Fig. S7h-i), which may result from Ra input from resuspended sediment; this latter pattern was also observed during AZ2 and AZ4 cruises (AmasSeds), indicating the relationship between the particulate and dissolved phases above the shelf is complex (Moore et al. 1995).

Estimate of apparent ages

Once radium isotopes are released into the dissolved phase, we assume that they behave conservatively and only dilution, mixing and radioactive decay change their concentration. Moore (2000a,b) established a method based on AR to estimate apparent ages (*t*) of coastal waters. To correct for mixing, $^{224}Ra_{ex}$ activity is normalized to ^{233}Ra activity thus allowing a better estimation of water ages than either isotope used alone. When both ^{223}Ra and ^{224}Ra activities are above the detection limit, this indicates that radium has been recently released from suspended particles. The time *t* elapsed between initial and observed AR can be calculated from the following expression:

$$\left[^{224}Ra_{ex}/^{223}Ra\right]_{obs} = \left[^{224}Ra_{ex}/^{223}Ra\right]_i \times e^{-t\lambda_{224}}/e^{-t\lambda_{223}} \quad (1)$$

where $[^{224}Ra/^{223}Ra]_i$ is the initial AR; $[^{224}Ra_{ex}/^{223}Ra]_{obs}$ is the AR for a given water sample; λ_{224} and λ_{223} are the decay constants for ^{224}Ra and ^{223}Ra, respectively.
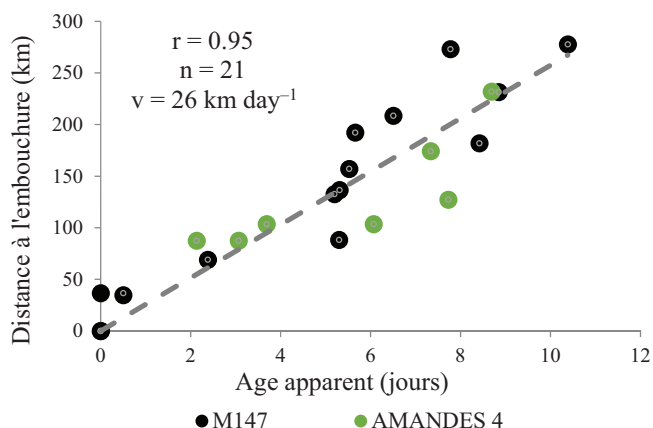
Fig. 5. Relationship between distance from the Amazon mouth (0.6°N, 49.7°W) and apparent ages determined along the Amazon plume that flows northward. On this plot, we selected data from M147 (in black) and AMANDES 4 (in green) that are plotted together. The slope of the best-fit linear regression gives the transport rate directly ($v = 26$ km d^{-1}).

t is thus the *apparent age* of the water sample that can be determined as follows:

$$t = \ln\left(\left[{}^{224}\mathrm{Ra}_{ex}/{}^{223}\mathrm{Ra}\right]_i / \left[{}^{224}\mathrm{Ra}_{ex}/{}^{223}\mathrm{Ra}\right]_{obs} \right) \times 1/(\lambda_{224} - \lambda_{223}) \tag{2}$$

This equation assumes (1) a single and constant value for the AR in the source region, (2) no addition or loss of Ra except for mixing and radioactive decay along the flow path, and (3) that the open ocean contains negligible excess of ^{223}Ra and ^{224}Ra (Moore 2000*a,b*). Because of the different assumptions associated with the age determination, we refer here to an apparent age of the water body instead of an absolute age.

In order to determine apparent ages along the Amazon plume, one has to define an initial AR. This is difficult because the initial AR may depend on different factors: ARs may change in relationship to the AR of the particles, which is related to the nature of the particles and potentially to the river discharge rate. Winds may also impact the residence time of the waters on the shelf (Limeburner et al. 1995) and may thus exert a control on the ARs. During prolonged periods of offshore winds from the east, water accumulates on the shelf. When the winds relax, water flows off the shelf. Tides may also play a role in the variability of the ARs. During spring tides, the vertical mixing increases, thus promoting the local resuspension of sediments especially at low depths. The periodicity of these events may cause changes in the initial AR.

We choose here to use the M147 cruise, which provides the highest sampling resolution in the Amazon mouth region, to determine the initial AR. We selected the nine stations in the Amazon mouth that display the highest AR (Fig. 3a). These samples display salinities <14. The mean AR thus obtained is

32.0 ± 2.3. Note that the highest AR (41) and two lower values determined in the Amazon mouth region (24.1 and 20.2) were excluded from the calculation after comparison with values found in the literature (Moore 2000*a*; Moore and Krest 2004; Peterson et al. 2008; Gu et al. 2012; Sanial et al. 2015). We used this AR to determine apparent ages along the plume. We applied the same AR to all Ra data because a proper initial AR was difficult to determine for the AZ4R and AMANDES cruises due to a lack of data near the mouth of the river. By doing so, we assumed that the initial AR was constant and was not changing over time (e.g., no change associated with the wind, seasons or the Amazon discharge rates). We recognize that the initial AR probably varies and by selecting the highest AR we may bias our ages on the high side, but the age trends should be consistent.

Note that Rousseau et al. (2015) reported the apparent ages derived from Ra isotopes during AMANDES 3 cruise using a different initial AR (i.e., 28.7 obtained during the AMANDES 3 cruise). By using an initial ratio slightly different to that used here (i.e., 32), the apparent ages thus obtained were slightly younger than those reported here; the difference, however, is on the order of a day, which is clearly within the age uncertainty. Therefore, this does not change the conclusions of Rousseau et al. (2015). As a comparison, the AR determined in the Oyapock River was 29.0 (this study), which is close to that reported here for the Amazon River.

Apparent ages of Amazon waters along the Brazilian shelf

The apparent ages increase with increasing distance from the Amazon mouth (Fig. 4). During AMANDES 3 cruise (Fig. 4b), the water sample closest to the Amazon mouth yields an apparent age of 3–5 d. The ages then gradually increase toward the east until reaching apparent ages of 10–12 d at the shelf break. Water samples collected during AMANDES 4 cruise also show increasing ages along the plume flow path toward the northwest (Fig. 4c). Apparent ages thus range between 2 and 11 d. We thus estimate that it takes approximately 10 d for the Amazon waters to reach the continental shelf of French Guiana.

Samples collected during AMANDES 1 cruise offshore French Guiana within the Amazon retroflexion also display decreasing apparent water ages with increasing distance from the coast (Fig. 4d). The samples collected near the Guiana coast display apparent ages (about 7–9 d) that could reflect the transport time needed between the Amazon mouth and French Guiana. Two samples located near the continental shelf during AMANDES 1 cruise have apparent ages (19 and 18 d) that do not follow this trend. These samples are characterized by relatively high salinities (35.2 and 36.4, respectively), suggesting that a complex mixing between different waters having different Ra sources may have obscured our apparent age estimates.

The higher sampling resolution of M147 allows us to construct maps of apparent ages with a higher spatial resolution
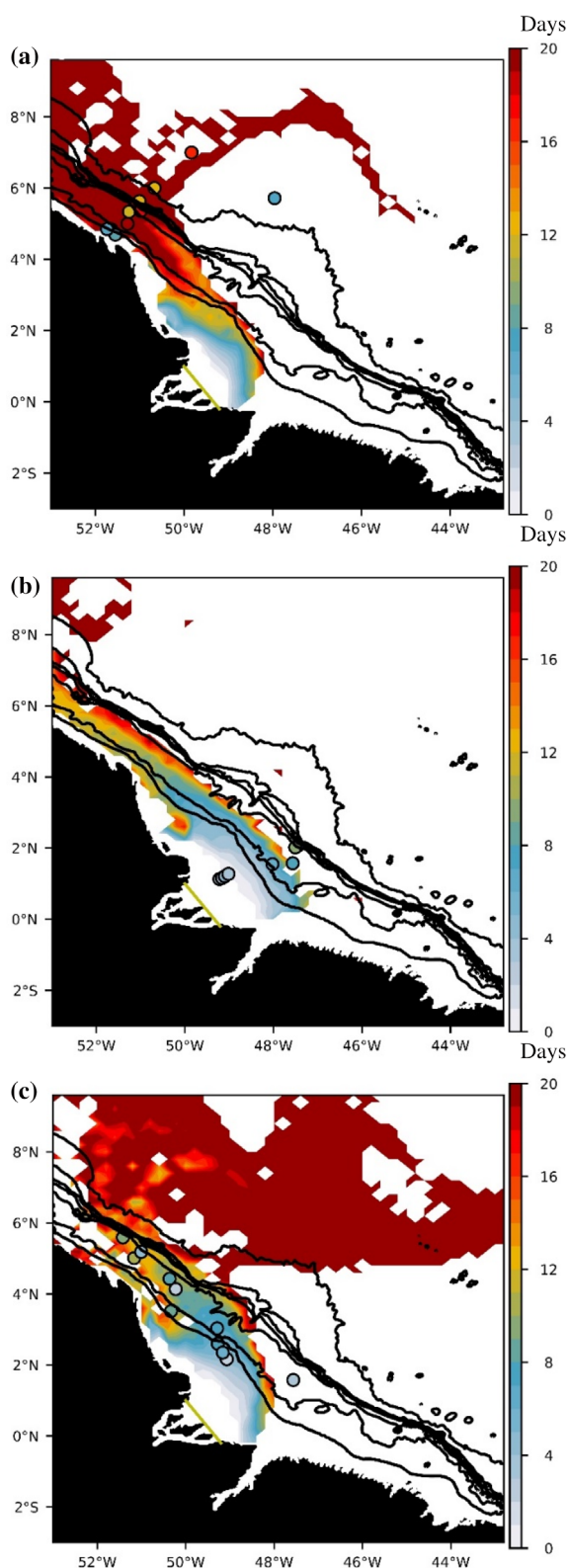
Fig. 6. Ages (in days) determined using NEMO model at the dates of AMANDES 1 (**a**), AMANDES 3 (**b**), and AMANDES 4 (**c**) cruises. The water parcels are released in the model along the green line but the age counter begins when the particles are in waters with a salinity >1. The colored circles show Ra apparent ages (days).

(Fig. 4a). In the first ~200 km in front of the Amazon mouth apparent ages range between 0 and 8 d and then increase toward the east and northwest. The Amazon plume is transported faster toward northwest (500 km in 11–14 d) than toward the east (250 km in 20 d). These observations agree with the circulation pattern in this area with the NBC flowing northeastward along the shelf. During M147 cruise, the Amazon waters reach the continental shelf of French Guiana after ca. 7–14 d (Fig. 4a), which is in good agreement with the observations during the AMANDES cruises (9–19 d).

Apparent ages determined during AZ4R cruise suggest that the Amazon waters reach the edge of the continental shelf after 9 d (Fig. 4e). On the shelf, the apparent ages range between 3 and 9 d but do not show a clear continuous trend (i.e., decrease with increasing distance from the mouth). Offshore the continental shelf, significant ^{223}Ra and ^{224}Ra activities were detected and the apparent ages range between 12 and 29 d. The offshore transect conducted during AZ4R cruise was designed to intersect the retroflected plume and thus did not follow the Amazon plume that is transported northward. Therefore, the apparent ages do not show a continuous decrease with increasing distance from the mouth. When the transect initially turned to the NW it ran against the Amazon plume, which had been redirected to the SE. The ages thus reflect punctual impacts of the Amazon waters on the offshore waters, as is also shown by the salinity data (Fig. 3e).

During the AmasSeds program, drifters were launched in the Amazon mouth shortly before AZ4R cruise. Figure 2 shows the track of one of these drifters and the stations occupied during AZ4R cruise. The cruise track was planned based on data received from the drifter. Ten days after the drifter was launched near Sta. 3, it had moved to 5°N on the mid shelf, where it entered the retroflexion. The cruise track aligned with the drifter path in the reverse direction. On day 21, the drifter was near Sta. 9 and near Sta. 7 on day 24. We calculated water ages of 23 d for Sta. 9 and 25 d for Sta. 7, in remarkable agreement with the history of the drifter.

The apparent ages determined at the edge of the French Guiana continental shelf range between 9 (AMANDES 4) and 14 d (M147). The apparent ages determined at the edge of the Brazilian shelf (east of the Amazon River) range between 12 (AMANDES 3) and 21 d (M147). These apparent ages determined at the edge of the continental shelf break allow us to estimate the residence time of the Amazon waters on the Brazilian continental shelf. We do not find any clear relationship between the discharge rate of the Amazon River and the residence time of the waters on the Brazilian continental shelf. Based on the data published by Lentz and Limeburner 1995) in the framework of the AmasSeds campaigns (1989–1991), Moore et al. (1995) estimated the residence time of the Amazon waters on the Brazilian continental shelf by combining the freshwater component on the shelf and the river flow and found a residence time of 12–23 d, which compares well with

the AR-based residence times (9–21 d in this study). Using drifters deployed during the same project, Limeburner et al. (1995) estimated a residence time of the Amazon waters in a range of 5–30 d.

Apparent velocity

Apparent water ages generally increase with increasing distance from the Amazon mouth. This pattern is illustrated in a relationship of apparent ages and salinity (Supplementary Information Fig. S8). In order to estimate the transport rate of the Amazon plume toward northwest, we selected data from AMANDES 4 and M147 cruises that are associated with the northwestward transport of the Amazon plume. Samples with salinities below 1.5 were excluded from the calculation in order to avoid cases where Ra would be essentially in the particular form. Following Moore and Krest (2004), we plotted the apparent ages as a function of salinity (Supplementary Information Fig. S8) and observed that at salinities greater than 25 (distance >300 km) the ages curve upward, as the mixing rate slows at higher salinity (Shiller 1993). Samples where salinities were above 25 were thus also excluded, as suggested by Moore and Krest (2004). The two datasets (AMANDES 4 and M147) do not show different relationships and therefore, they are plotted together.

The resulting relationship between distance from the river mouth and apparent ages shows a linear regression (Fig. 5; $r = 0.95$; $n = 21$). The slope of the linear regression provides an estimate of the apparent transport rate of 26 km d^{-1} or 30 cm s^{-1}. In this latter calculation, the distances from the mouth have been determined from a straight line and thus do not consider the potential complex water flow paths on the continental shelf. The apparent transport rate reported here may thus be a minimum estimate.

During the AMANDES project, a mooring was deployed at the continental shelf, which recorded the transport rate of the northwestward current at 10 m depth (location 1.1°N, 46.7°W at the 50 m isobaths). Highly temporal variable transport rates were observed with a maximum value up to 100 cm s^{-1} and a minimum value when currents are flowing toward southeast (Prestes et al. 2018). Drifters launched at the Amazon mouth during AmasSeds program revealed transport rates in the range of 41–128 cm s^{-1} (Limeburner et al. 1995). These authors indicated a significant acceleration of the current at 2°N between the 5 and 20 m isobaths due to sharp variations of the bathymetry in this area. Note that the apparent transport rate estimate derived from Ra isotopes integrates observations conducted over 300 km distance. The spatial and temporal timescales are thus different when compared to moorings, which provide information at one single location. Finally, Moore et al. (1995) arrived at a transport velocity higher than 80 cm s^{-1} in order to explain the Ra isotope distribution in July and September 1989 between the Amazon shelf and

offshore French Guiana. We do not find a clear relationship between the discharge rates of the Amazon River and the residence time of the waters on the Brazilian continental shelf. This is consistent with previous observational and modeling studies, which suggest that circulation on the shelf is driven at first order by tides and the wind-driven circulation (Geyer 1995; Lentz 1995; Nikiema et al. 2007; Ruault et al. 2020).

Modeling

The Lagrangian trajectories obtained from the regional simulation were used to generate water ages above the continental shelf at the time of the three AMANDES campaigns. Ages have been averaged over the periods of the different campaigns and are shown in Fig. 6, together with apparent ages determined from Ra isotopes.

The AMANDES 1 samples were collected within the Amazon retroflexion, except for one sample (6°N, 48°W) where the value is not comparable to the model (Fig. 6a). Two samples near the Guiana coast show younger ages than those predicted by the model, but the lack of statistics at the edge of the plume, error associated with the model, the shallow depth and the proximity of the Oyapock River may influence these data. Two samples further away from the coast (with ages of 19 and 18 d; red color in Fig. 6a) display ages similar to the ages derived from the model. Within the retroflexion, three Ra ages are slightly younger than the model ages (yellow color; Fig. 6a). The ages calculated from radium data during the AMANDES 3 campaign (Fig. 6b) are in good agreement with the ages calculated by the model, except for the two samples collected at the shelf edge that display ages slightly younger than the model ages. Regarding the AMANDES 4 campaign (Fig. 6c), the Ra ages are in good agreement with the model up to 4°N. Offshore the French Guiana coast, the ages derived from Ra isotopes appear to be slightly younger than the model age.

Overall, considering the uncertainties on the Ra ages (at least 1 to 3 d) and on the model ages, we conclude that the global good agreement between the two methods validates the model. We note that the Ra ages sometimes appear to be younger than the model ages in offshore waters, a pattern that may be explained by the relatively low ^{223}Ra and ^{224}Ra activities, which may complicate the age calculation in these samples, using the method developed by Moore (2000b).

Conclusion

We summarized a unique dataset acquired during five different campaigns conducted offshore the Amazon mouth and used Ra isotopes (^{223}Ra and ^{224}Ra) to determine apparent ages of the Amazon plume. The apparent ages thus determined are in relatively good agreement with the ages determined using a high-resolution numerical simulation based on the NEMO 3.6 ocean model, which suggests that, except for decay, Ra behaves conservatively along the plume and that the

assumptions used to derive Ra the apparent ages are likely valid. Alternatively, apparent ages calculated from Ra in situ data validate the model.

Our results suggest that it takes 9–14 d for the Amazon waters to reach the French Guiana continental shelf and between 12 and 21 d to reach the edge of the Brazilian shelf (east of the Amazon River). We thus calculate a gross transport rate of ~30 cm s^{-1} for the Amazon waters that flow toward the Northwest, when the retroflexion is not active. This method has the great advantage of providing an integrated estimate that includes data from the entire continental shelf, in contrast to estimates derived from current meters moored at a very localized spot. We do not find any clear relationship between the discharge rate of the Amazon River and the residence time of the waters on the Brazilian continental shelf. Combining the information obtained from Ra isotopes with the elemental distributions on the shelf will allow us in future studies to provide the timescale of chemical reactions that take place along the salinity gradient and to derive the chemical fluxes transported toward offshore waters.

References

Armijos, E., and others. 2020. Rainfall control on Amazon sediment flux: Synthesis from 20 years of monitoring. Environ. Res. Commun. **2**: 051008. doi:10.1088/2515-7620/ab9003

Baklouti, M., J.-L. Devenon, A. Bourret, J.-M. Froidefond, J.-F. Ternon, and J.-L. Fuda. 2007. New insights in the French Guiana continental shelf circulation and its relation to the North Brazil current retroflection. J. Geophys. Res. **112**: C02023. doi:10.1029/2006JC003520

Blanke, B., and S. Raynaud. 1997. Kinematics of the Pacific equatorial undercurrent: An Eulerian and Lagrangian approach from GCM results. J. Phys. Oceanogr. **27**: 1038–1053.

Cabral, A., T. Dittmar, M. Call, J. Scholten, C. E. de Rezende, N. Asp, M. Gledhill, M. Seidel, and I. R. Santos. 2021. Carbon and alkalinity outwelling across the groundwater-creek-shelf continuum off Amazonian mangroves. Limnol. Oceanogr. Lett. **6**: 369–378.

Callède, J., G. Cochonneau, F. V. Alves, J.-L. Guyot, V. S. Guimarães, and E. De Oliveira. 2010. Les apports en eau de l'Amazone à l'Océan Atlantique. Rev. Sci. Eau **23**: 247–273. doi:10.7202/044688ar

Coles, V., M. T. Brooks, J. Hopkins, M. R. Stukel, P. L. Yager, and R. R. Hood. 2013. The pathways and properties of the Amazon River plume in the tropical North Atlantic Ocean. J. Geophys. Res. Oceans **20**: 8981. doi:10.1002/2013JC008981

Dai, A., and K. E. Trenberth. 2002. Estimates of frshwater discharge from continents: Latitudinal and seasonal variations. J. Hydrometeorol. **3**: 660–687.

Demaster, D. J., and R. H. Pope. 1996. Nutrient dynamics in Amazon shelf waters: results from AMASSEDS. Cont. Shelf Res. **16**: 263–289. doi:10.1016/0278-4343(95)00008-O

Dussin, R., B. Barnier, L. Brodeau 2016. Up-dated description of the DFS5 forcing data set: The making of Drakkar forcing set DFS5, DRAKKAR/MyOcean Rep. Lab Glaciol Env. Geophys Grenoble Fr.

Garcia-Solsona, E., J. Garcia-Orellana, P. Masqué, and H. Dulaiova. 2008. Uncertainties associated with 223Ra and 224Ra measurements in water via a delayed coincidence counter (RaDeCC). Mar. Chem. **22**: 198–219.

Geyer, W. R. 1995. Tide-induced mixing in the Amazon frontal zone. J. Geophys. Res. **100**: 2341. doi:10.1029/94JC02543

Geyer, W. R., and G. C. Kineke. 1995. Observations of currents and water properties in the Amazon frontal zone. J. Geophys. Res. **100**: 2321. doi:10.1029/94JC02657

Geyer, R. W., R. C. Beardsley, S. J. Lentz, J. Candela, R. Limeburner, W. E. Johns, B. M. Castro, and I. Dias Soares. 1996. Physical oceanography of the Amazon shelf. Cont. Shelf Res. **16**: 575–616. doi:10.1016/0278-4343(95)00051-8

Gibs, R. J. 1972. Water chemistry of the Amazon River. Geochim. Cosmochim. Acta **36**: 1061–1066. doi:10.1016/0016-7037(72)90021-X

Grodsky, S. A., N. Reul, G. Lagerloef, G. Reverdin, J. A. Carton, B. Chapron, Y. Quilfen, V. N. Kudryavtsev, and H.-Y. Kao. 2012. Haline hurricane wake in the Amazon/Orinoco plume: AQUARIUS/SACD and SMOS observations. Am. Geophys. Union **9**: 53335. doi:10.1029/2012GL053335

Gu, H., W. S. Moore, L. Zhang, J. Du, and J. Zhang. 2012. Using radium isotopes to estimate the residence time and the contribution of submarine groundwater discharge (SGD) in the Changjiang effluent plume, East China Sea. Cont. Shelf Res. **35**: 95–107. doi:10.1016/j.csr.2012.01.002

Hu, C., E. Montgomery, R. Schmitt, and F. Mullerkarger. 2004. The dispersal of the Amazon and Orinoco River water in the tropical Atlantic and Caribbean Sea: Observation from space and S-PALACE floats. Deep Sea Res Part II Top. Stud. Oceanogr. **51**: 1151–1171. doi:10.1016/S0967-0645(04)00105-5

HYBAM, 2020. Contrôles géodynamique, hydrologique et biogéochimique de l'érosion/altération et des transferts de matière dans les bassins de l'Amazone, de l'Orénoque et du Congo. [accessed 2020 February 22]. Available from http://www.ore-hybam.org.

Ibánhez, J. S. P., M. Araujo, and N. Lefèvre. 2016. The overlooked tropical oceanic CO_2 sink: Overlooked tropical oceanic CO_2 sink. Geophys. Res. Lett. **43**: 3804–3812. doi:10.1002/2016GL068020

Johns, W. E., T. N. Lee, F. A. Schott, R. J. Zantopp, and R. H. Evans. 1990. The North Brazil current retroflection seasonal structure and eddy variability. J. Geophys. Res. **95**: 22,103–22,120. doi:10.1029/JC095iC12p22103

Johns, W. E., T. N. Lee, R. C. Beardsley, J. Candela, R. Limeburner, and B. Castro. 1998. Annual cycle and variability of the North Brazil current. J. Phys. Oceanogr. **28**: 26.

Key, R. M., R. F. Stallard, W. S. Moore, and J. L. Sarmiento. 1985. Distribution and flux of ^{226} Ra and ^{228} Ra in the Amazon River estuary. J. Geophys. Res. **90**: 6995. doi:10.1029/JC090iC04p06995

Kineke, G. C., R. W. Sternberg, J. H. Trowbridge, and W. R. Geyer. 1996. Fluid-mud processes on the Amazon continental shelf. Cont. Shelf Res. **16**: 667–696. doi:10.1016/0278-4343(95)00050-X

Kuehl, S. A., D. J. DeMaster, and C. A. Nittrouer. 1986. Nature of sediment accumulation on the Amazon continental shelf. Cont. Shelf Res. **6**: 209–225. doi:10.1016/0278-4343(86)90061-0

Le Bars, Y., F. Lyard, C. Jeandel, and L. Dardengo. 2010. The AMANDES tidal model for the Amazon estuary and shelf. Ocean Model. **31**: 132–149. doi:10.1016/j.ocemod.2009.11.001

Lefévre, N., D. Diverrés, and F. Gallois. 2010. Origin of CO_2 undersaturation in the western tropical Atlantic. Tellus B Chem. Phys. Meteorol. **62**: 595–607. doi:10.1111/j.1600-0889.2010.00475.x

Lentz, S. J. 1995. The Amazon River plume during AMASSEDS: Subtidal current variability and the importance of wind forcing. J. Geophys. Res. **100**: 2377–2390. doi:10.1029/94JC00343

Lentz, S. J., and R. Limeburner. 1995. The Amazon River plume during AMASSEDS: Spatial characteristics and salinity variability. J. Geophys. Res. **100**: 2355. doi:10.1029/94JC01411

Limeburner, R., R. C. Beardsley, I. D. Soares, S. J. Lentz, and J. Candela. 1995. Lagrangian flow observations of the Amazon River discharge into the North Atlantic. J. Geophys. Res. **100**: 2401. doi:10.1029/94JC03223

Livingstone, D.A. 1963. Chemical composition of rivers and lakes. US Geol. Surv. Prof. Pap. 1–63.

Madec, G. 2014. "NEMO ocean engine" (Draft edition r5171), Note du Pôle Modélisation 27, Inst. Pierre-Simon Laplace, France, ISSN No 1288-1619.

Meade, R. H., T. Dunne, J. E. Richey, D. M. Santos, and E. Salati. 1985. Storage and remobilization of suspended sediment in the lower Amazon River of Brazil. Science **228**: 488–490. doi:10.1126/science.228.4698.488

Moore, W. S., and D. F. Reid. 1973. Extraction of radium from natural waters using manganese-impregnated acrylic fibers. J. Geophys. Res. **78**: 8880–8886. doi:10.1029/JC078i036p08880

Moore, W. S. 1976. Sampling 228Ra in the deep ocean. Deep Sea Res. Oceanogr. Abstr. **23**: 647–651. doi:10.1016/0011-7471(76)90007-3

Moore, W. S., J. L. Sarmiento, and R. M. Key. 1986. Tracing the Amazon component of surface Atlantic water using 228Ra, salinity and silica. J. Geophys. Res. **91**: 2574. doi:10.1029/JC091iC02p02574

Moore, W. S., and J. F. Todd. 1993. Radium isotopes in the Orinoco estuary and eastern Caribbean Sea. J. Geophys. Res. Oceans **98**: 2233–2244. doi:10.1029/92JC02760

Moore, W. S., H. Astwood, and C. Lindstrom. 1995. Radium isotopes in coastal waters on the Amazon shelf. Geochim. Cosmochim. Acta **59**: 4285–4298. doi:10.1016/0016-7037(95)00242-R

Moore, W. S., and R. Arnold. 1996. Measurement of ^{223} Ra and ^{224} Ra in coastal waters using a delayed coincidence counter. J. Geophys. Res. Oceans **101**: 1321–1329. doi:10.1029/95JC03139

Moore, W. S., D. J. DeMaster, J. M. Smoak, B. A. McKee, and P. W. Swarzenski. 1996. Radionuclide tracers of sediment-water interactions on the Amazon shelf. Cont. Shelf Res. **16**: 645–665. doi:10.1016/0278-4343(95)00049-6

Moore, W. S. 2000 *a*. Ages of continental shelf waters determined from ^{223} Ra and ^{224} Ra. J. Geophys. Res. Oceans **105**: 22117–22122. doi:10.1029/1999JC000289

Moore, W. S. 2000 *b*. Determining coastal mixing rates using radium isotopes. Cont. Shelf Res. **20**: 1993–2007. doi:10.1016/S0278-4343(00)00054-6

Moore, W. S., and J. Krest. 2004. Distribution of 223Ra and 224Ra in the plumes of the Mississippi and Atchafalaya Rivers and the Gulf of Mexico. Mar. Chem. **86**: 105–119. doi:10.1016/j.marchem.2003.10.001

Moore, W. S. 2008. Fifteen years experience in measuring 224Ra and 223Ra by delayed-coincidence counting. Mar. Chem. **109**: 188–197. doi:10.1016/j.marchem.2007.06.015

Muller-Karger, F. E., C. R. McClain, and P. L. Richardson. 1988. The dispersal of the Amazon's water. Nature **333**: 56–59. doi:10.1038/333056a0

Müller-Karger, F. E., C. R. McClain, T. R. Fisher, W. E. Esaias, and R. Varela. 1989. Pigment distribution in the Caribbean Sea: Observations from space. Prog. Oceanogr. **23**: 23–64. doi:10.1016/0079-6611(89)90024-4

Nikiema, O., J.-L. Devenon, and M. Baklouti. 2007. Numerical modeling of the Amazon River plume. Cont. Shelf Res. **27**: 873–899. doi:10.1016/j.csr.2006.12.004

Nittrouer, C. A., T. B. Curtin, and D. J. DeMaster. 1986. Concentration and flux of suspended sediment on the Amazon continental shelf. Cont. Shelf Res. **6**: 151–174. doi:10.1016/0278-4343(86)90058-0

Nittrouer, C. A., S. A. Kuehl, R. W. Sternberg, A. G. Figueiredo, and L. E. C. Faria. 1995. An introduction to the geological significance of sediment transport and accumulation on the Amazon continental shelf. Mar. Geol. **125**: 177–192. doi:10.1016/0025-3227(95)00075-A

Nittrouer, C. A., and D. J. DeMaster. 1996. The Amazon shelf setting: Tropical, energetic, and influenced by a large river. Cont. Shelf Res. **16**: 553–573. doi:10.1016/0278-4343(95)00069-0

Peterson, R. N., W. C. Burnett, M. Taniguchi, J. Chen, I. R. Santos, and S. Misra. 2008. Determination of transport rates in the Yellow River–Bohai Sea mixing zone via natural

geochemical tracers. Cont. Shelf Res. **28**: 2700–2707. doi:10.1016/j.csr.2008.09.002

Prestes, Y. O., A. C. d. Silva, and C. Jeandel. 2018. Amazon water lenses and the influence of the North Brazil current on the continental shelf. Cont. Shelf Res. **160**: 36–48. doi:10.1016/j.csr.2018.04.002

Reul, N., Y. Quilfen, B. Chapron, S. Fournier, V. Kudryavtsev, and R. Sabia. 2014. Multisensor observations of the Amazon-Orinoco River plume interactions with hurricanes. J. Geophys. Res. **119**: 8271–8295. doi:10.1002/2014JC010107

Rousseau, T. C. C., J. E. Sonke, J. Chmeleff, P. van Beek, M. Souhaut, G. Boaventura, P. Seyler, and C. Jeandel. 2015. Rapid neodymium release to marine waters from lithogenic sediments in the Amazon estuary. Nat. Commun. **6**: 7592. doi:10.1038/ncomms8592

Ruault, V., J. Jouanno, F. Durand, J. Chanut, and R. Benshila. 2020. Role of the tide on the structure of the Amazon plume: A numerical modeling approach. J. Geophys. Res. Oceans **125**: 15495. doi:10.1029/2019JC015495

Sanial, V., P. van Beek, B. Lansard, M. Souhaut, E. Kestenare, F. d'Ovidio, M. Zhou, and S. Blain. 2015. Use of Ra isotopes to deduce rapid transfer of sediment-derived inputs off Kerguelen. Biogeosciences **12**: 1415–1430. doi:10.5194/bg-12-1415-2015

Shiller, A. M. 1993. A mixing rate approach to understanding nutrient distributions in the plume of Mississippi River. Mar. Chem. **43**: 211–216. doi:10.1016/0304-4203(93)90226-E

Smith, W. O., and D. J. Demaster. 1996. Phytoplankton biomass and productivity in the Amazon River plume: Correlation with seasonal river discharge. Cont. Shelf Res. **16**: 291–319. doi:10.1016/0278-4343(95)00007-N

Smoak, J. M., D. J. DeMaster, S. A. Kuehl, R. H. Pope, and B. A. McKee. 1996. The behavior of particle-reactive tracers in a high turbidity environment: 234Th and 210Pb on the Amazon continental shelf. Geochim. Cosmochim. Acta. **60**: 2123–2137. doi:10.1016/0016-7037(96)00092-0

Sun, Y., and T. Torgersen. 1998. The effects of water content and Mn-fiber surface conditions on measurement by emanation. Mar. Chem. **62**: 299–306. doi:10.1016/S0304-4203(98)00019-X

Conflict of interest

None declared.